Investigation of Impact of Ceramic Nanomaterial Addition on Ductile Minerals: A Powder Metallurgy Approach

Nada Mansoor HASSAN¹, Salih Younis DARWEESH^{2*}, Ashwaq Tariq DAHHAM³

¹ Physics Department, College of Pure Science, Kirkuk University, Al-Sayada, Kirkuk, 36001, Iraq

Received 16 June 2025; accepted 11 September 2025

The addition of ceramic nanomaterials has a clear effect on minerals that suffer from ductility, when silica (SiO₂) is incorporated into nickel metal (Ni) in volume ratios of 2 %, 4 %, 6 %, 8 %, and 10 %. The powder metallurgy process involved mixing designated volume ratios, the powders are milled for two hours using a custom electric mixer. Subsequently, the powder is placed into a press mold with a diameter of 10 mm, and the pressing operation is executed using a hydraulic press at a pressure of (80 MPa) for one minute. The resulting samples were heated at (1100 °C) for two hours. Some tests were conducted before and after the thermal sintering process, and the thermal treatments yielded significant experimental results, with the Brinell method showing the highest hardness at 770 kg/mm² and the best compressive strength at 68 MPa. Additionally, the lowest porosity recorded was 9 %. Regarding the structural findings, the scanning electron microscopy (SEM) and X-ray diffraction provided clear results for the fabricated models in terms of how the structural elements were connected and dependent on each other, as well as the characteristics of the reinforcing material and its ability to permeate through the surface of the nickel base material.

Keywords: nanomaterials, structural properties, hardness, cermet.

1. INTRODUCTION

The advanced engineering materials used in industrial technological applications varied [1]. Among these, advanced ceramics such as SiO2 and Al2O3 are particularly noteworthy due to their exceptional hardness [2]. Various methods are used to produce these materials, with powder technology being the most significant one [3]. The field of composite materials is very complex and can't be understood just by knowing the basic principles or standard conditions [4]. It is important to emphasize that the research in this area aims to identify composite materials that can be used in various conditions and enhance the properties of materials with a weak structure [5]. Moreover, the fundamental principles should be complemented by a strong emphasis on practical applications [6], reflecting the dual objectives of minimizing costs while maximizing material specifications [7]. Specifically, the materials under investigation are nano-reinforced metals that exhibit high strength-to-weight and stiffness-to-weight ratios [8] which are now crucial in weight-sensitive industries like aircraft and spacecraft [9]. Composite materials now play a major role in the construction of modern vehicles and tools [10]. They have also expanded into urban construction, including tall buildings, bridge bases, and other components [11], [12]. Their high resistance to erosion, corrosion, heat, and high temperatures has made them an essential part of modern life [13]. The key distinguishing factor of composite materials is their base phase of metal and a reinforced phase, which may consist of a nano-ceramic material. This design allows the material to withstand and absorb shocks

effectively [16]. The primary phase has continuity and is typically longer, more durable, and less rigid. It can be composed of metals, plastics, or ceramics. [17-19]. Metals and plastics can be used as basic phases [20], due to their possession of some ductility, which is one of the preferred properties [21]. As for the ceramic phase, the added reinforcement is in order to improve the crack toughness [22]. The primary phase involves one or multiple materials [23]. One of its key features is the presence of reinforcement phases [24] and the distribution of applied stresses [25]. The primary phase may contain either the phase or the supported secondary phases, which are commonly referred to as the strengthening or reinforcement phase. This phase is known for its high strength and hardness [26, 27]. The main purpose of the supported phase is to provide the best levels of hardness and resistivity of composite materials [28]. Many common materials (metallic alloys, ceramics and plastics mixed with additives) [29], have small amounts of phases dispersed in their structure [30], but are not considered composite materials since its physical properties are similar to those of the basic phases [31] yet, the physical properties of steel are similar to the properties of pure iron

2. AIM OF THE WORK

The article aims to improve the mechanical and structural properties of nickel by adding nano-silica oxide, which has distinctive physical properties.

² Physics Department, College of Science, Tikrit University, Al-Jamia, Tikrit, 34001, Iraq

³ Physics Department, College of Science for Women, Baghdad University, Al-Jadriya, Baghdad, 10071, Iraq http://doi.org/10.5755/j02.ms.41899

^{*} Corresponding author: S.Y. Darweesh E-mail: Salih.younis@tu.edu.iq

3. BASIC MATERIALS USED

Nickel metal Ni is used as a base material and manufactured by Sulzer Metco (Swiss) with a purity of 99.5 %, while the nano-support material was silica SiO_2 from Changsha Santech Co.) of (Chinese) origin with a purity of 99.8 %. The grain size of Nickel was 75 μ m, while silica's was 35 nm.

4. METHOD

The electric mixer is used to mix metal-based powders, such as nickel (Ni), at varying volumetric ratios (98 %, 96 %, 94 %, 92 %, 90 %), along with nano-silica material SiO₂ at volumetric ratios (2 %, 4 %, 6 %, 8 %, 10 %). Volumetric ratios are adjusted based on the difference in densities between the support material and the base material [33]. Once the mixing process is finished, both mixtures undergo a brief heat treatment at 100 °C for half an hour. The hydraulic press used is a HALIM USTA model of Turkish origin, with a maximum load capacity of 20 tons. Fig. 1 shows the mold used. The pressure applied to all the prepared models is 80 MPa for one minute during the pressing process. It usually suffers from softness or the socalled green density, and therefore it needs a thermal sintering process, which was carried out using a type (Muffle Furnace) of Korean origin and model 12-MF, with a maximum temperature of (1200 °C), where the samples were sintered at a temperature (1100 °C) for two hours only. The sintering temperature was chosen to ensure that the sintering degree falls within the range of 70-90 % of the base material's melting point [34]. Approximately 76 % of nickel's melting point was used, taking into account the availability of the laboratory furnace. Once the samples are finished in the furnace, they are thoroughly cleaned and prepared for mechanical and chemical tests.



Fig. 1. The mold used for pressing powders [1]

5. STRUCTURAL AND PHYSICAL TESTS

5.1. Scanning electron microscope

The scanning electron microscope is a crucial tool for evaluating surface topography, examining structure, and measuring particle size. Additionally, it can determine the proportions of elements within a compound using energy-dispersive X-ray spectroscopy (EDX). In this study, a Belgian-origin scanning electron microscope (MIRA TESCAN) was utilized to direct an electron beam onto the

sample's surface, producing signals that reveal information about its shape and topography [35]. The benefit of the EDX test is to identify and confirm the elemental composition and distribution in the composite, supporting phase verification and dispersion assessment. a Belgian-origin EDX (MIRA TESCAN).

5.2. X-ray diffraction

The purpose of X-ray diffraction analysis is to determine the fundamental components of the alloy, as well as the phases and crystalline structures that are formed. X-ray diffraction of the samples was performed using an Aeris Research device manufactured by Malvern Panalytical, a Dutch company. The tube used was a Cu k α diffract meter, and the test was carried out at room temperature. This non-destructive examination method helps identify the chemical and physical properties of the materials used. The angle of the X-rays hitting the material is crucial in determining the basis of the diffraction work, and it is dependent on a specific angle of incidence [36]. Bragg's equation is used to describe the diffraction condition, as shown in the following Eq. 1 [37].

$$n\lambda = 2d\sin\theta,\tag{1}$$

where n is an integer representing the order of the diffraction peak; λ is the wavelength of the x-ray; θ is the diffraction angle.

5.3. Porosity

Porosity is the preferred measure for analyzing certain packing properties of powders. It is defined as the ratio of pores in powders to the bulk volume of the sample. Several factors, such as granule shape, size and distribution, and bonding strength, can influence porosity significantly. An increase in the fine granules relative to the coarse granules means a decrease in the porosity [39]. The pressure used for formation affects the proportion of the pores [40] because the use of high pressure will lead to an increase in the compaction of the granules and a decrease in the porosity. For instance, when the model is sintered at a high temperature, materials with low melting points will melt and fill the pores in the structure, resulting in a decrease in porosity. The percentage of the real porosity can be measured through the following relationship Eq. 2 [41]:

T. P. % =
$$\frac{\text{T.D.-B.D.}}{\text{T.D.}} \times 100 \%$$
, (2)

where T.P. is the total porosity ratio of the sample; B.D. is the density of the sample in practice (The density of the body); T.D. is the theoretical density in g/cm³.

5.4. Brinell hardness test

To measure the hardness of the prepared samples, we used a Swedish-made programmed hardness device (type (2) Proced Equotip) with the reflux method. The device can directly display hardness values on its screen. It is capable of converting hardness values from one method to another. The device is programmed to provide the specific Brinell hardness numbers used in this research. Table 1 displays the key features of the device used. Brinell hardness (HB) can be determined using the following Eq. 3 [42]:

HB = F/
$$\left(\frac{1}{2}\right)\pi D(D - \sqrt{D^2 - d^2})$$
, (3)

where D is the diameter of the ball in mm; d is the diameter of the circular trace in mm; F is the applied load in kg.

Table 1. Shows the most important characteristics of the device used

No.	Title	Values
1	Maximum hardness	940 HV
2	Impact energy	11 Nm
3	Mass of the impact body	5.5 g
4	Diameter test tip	3 mm
5	Diameter impact device	20 mm
6	Length impact service	150 mm

5.5. Diametral compressive strength

The compressive strength provides the maximum load that the material can bear before failure, and the compressive strength is a design factor when manufacturing composite materials [43]. The ability of a material to resist compression failure is influenced by the way the load is applied and the dimensions of the sample being tested. According to international standards, the height of the sample should not exceed its diameter when testing compressive strength. However, producing samples with heights close to their diameter can be challenging and expensive. The test has some restrictions. It can cause flexural stress and friction due to the increased surface area of the sample being tested, which can affect the test results.

As a result, cylindrical composite materials are tested by applying continuous loads to the sample's diameter until it fails [44]. A resistance value can be found by compression σ from the following Eq. 4 [45]:

$$\sigma = \frac{2*F}{\pi h d_S},\tag{4}$$

where ds is the sample diameter in mm; h is the sample height in mm; F is the maximum projected load in N.

6. RESULTS AND DISCUSSION

6.1. Scanning electron microscope results

Encouraging results are obtained from the scanning electron microscope, which was carried out at a depth of 2 µm and with a magnification of 15 KX. Fig. 2 shows SEM the thermal sintering process. Fig. 2 a displays a nanosupport ratio of 2, revealing the entanglement and crystalline coordination between the base material and support material, as well as the distribution of silica across the nickel surface. In contrast, Fig.2 b with a nano-support rate of 4 % shows an amplified spread of the support material, yet it also exhibits some crystalline defects on the surface. Regarding Fig. 2 c, when cementing with a 6 % nano-silica reinforcement, we observe that the pores and crystalline defects remain, but the spread of nano-silica is visible in white across the surface.

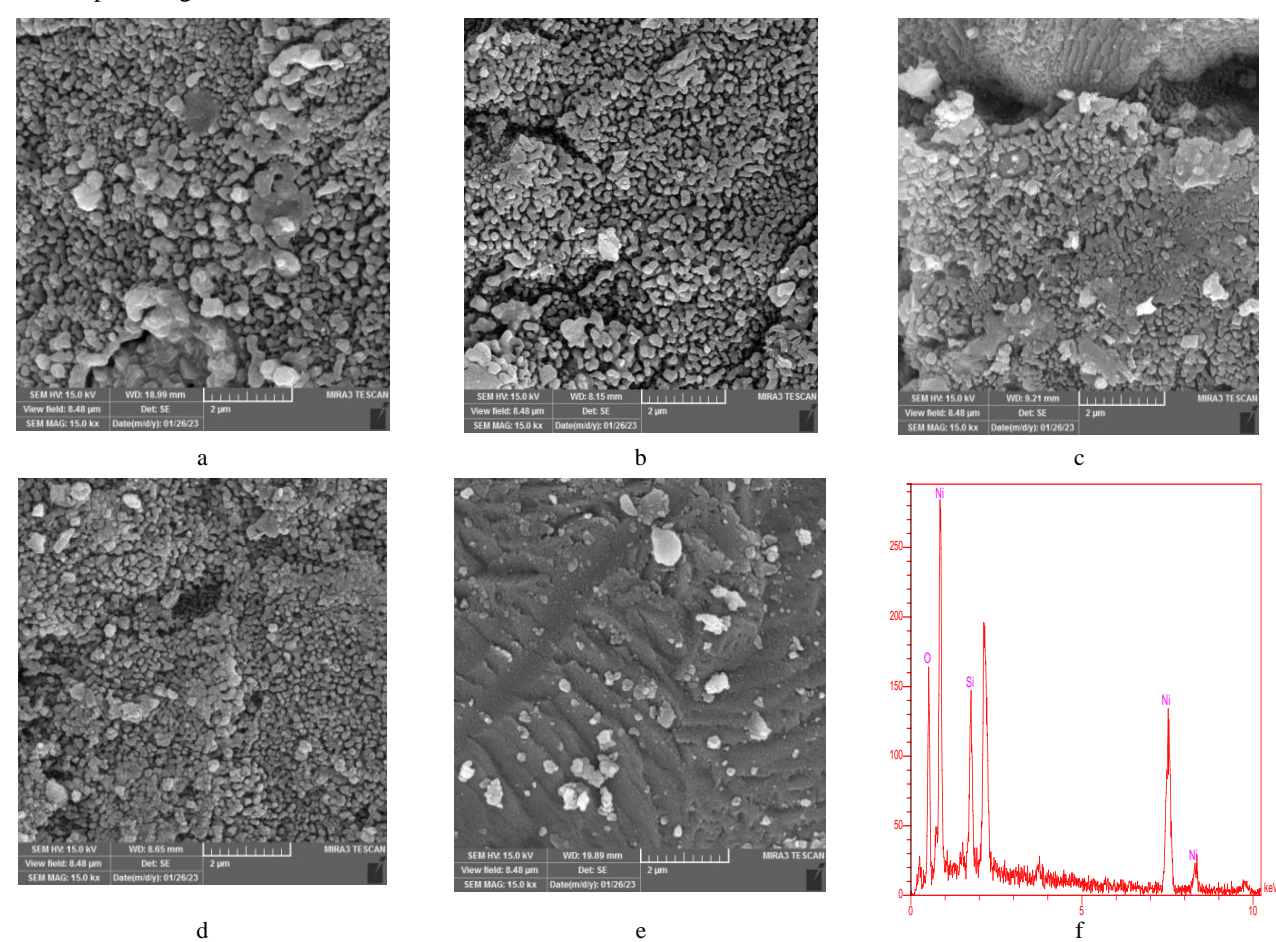


Fig. 2. Shows electronic images of (Ni-SiO₂) composites at different reinforcement ratios: a−2%; b−4%; c−6%; d 8%; e−10%; f−EDX spectrum after the thermal sintering process

In Fig. 2 d with an 8 % reinforcement rate, we notice a reduction in crystalline defects and an enhancement in the mechanical interlocking of the two mixtures. Meanwhile, at a 10 % nano reinforcement ratio, Fig. 2 e displays a surface that is almost free of pores, cracks, and other crystalline defects. We observed silica dispersed throughout the nickel base material, suggesting that the optimal mixing ratio achieved is 90 % Ni-10 % SiO₂. This results in nanomaterial properties that enhance hardness, minimize porosity, and alleviate stress by disrupting the arrangement of nickel atoms. Consequently, a cermet alloy is produced with characteristics that blend the strength and cohesion of nanomaterials with the ductility and cohesion of metal [46, 47].

6.2. X-ray diffraction results

X-ray diffraction patterns are a crucial test in materials science for identifying the materials used and determining the resulting crystal structures following mixing and pressing. Fig. 3 displays the X-ray diffraction of the (Ni-SiO₂) compounds after the sintering process and at various support ratios of nano-silica 2, 4, 6, 8, 10%.

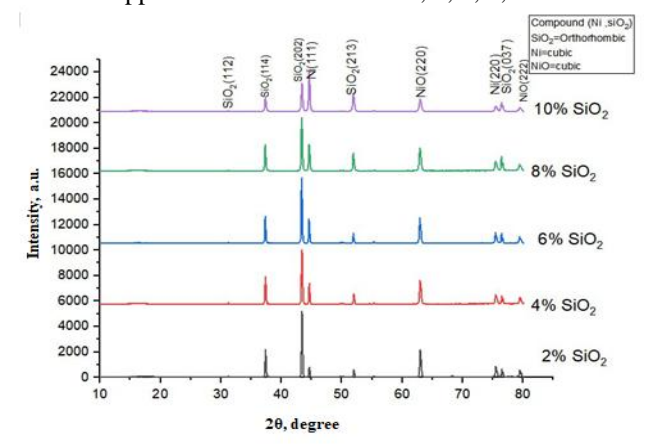


Fig. 3. X-ray diffraction patterns XRD of Ni-%SiO₂ composites at different reinforcement ratios

As shown in Fig. 3, the nano-silica material (SiO₂) was observed to have a rhombic crystal system (orthorhombic) with main angles at $2\theta = 37, 44, 53, 77$. Meanwhile, the base metal nickel exhibited a cubic system (Cubic) with crystal angles at $2\theta = 45,76$. Additionally, due to the interaction of oxygen with nickel during thermal sintering processes, nickel oxide (NiO) was found to have a cubic system (Cubic) with crystal angles at $2\theta = 63.5$, 80. Nickel oxide's presence, along with nanoscale silicon oxide, created an alloy with unique mechanical and physical properties. This is due to the high hardness of nickel oxide, which has various industrial applications such as in ceramic materials [48] and casting. It also finds use in nickel alloys [49] and fuel cells as an electrode [50]. These applications contribute to the mechanical properties of composites, especially when a certain percentage of silica support is involved.

6.3. Real porosity results

Fig. 4 illustrates the correlation between the percentages of nano-silica added and the real porosity after thermal sintering at 1100 °C for two hours. It is evident that

there is a significant relationship between porosity and hardness. With an increase in the percentage of nickel metal support material, the porosity decreases, reaching its lowest value of 17 % before sintering with 10 % reinforcement material. After sintering, the porosity decreases further to 9 % at the same reinforcement percentage of 10 %.

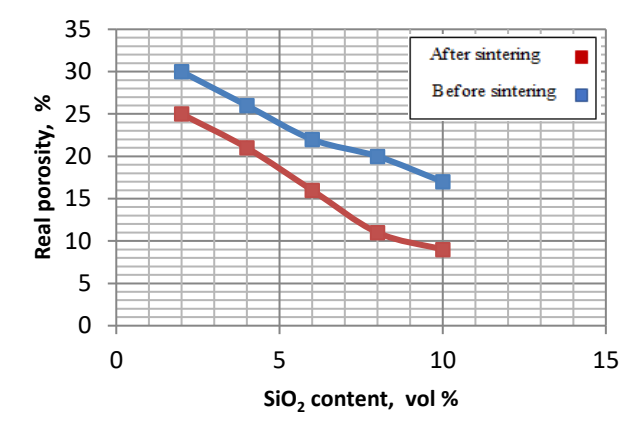


Fig. 4. The relationship between the reinforcement volumetric ratios and the real porosity before and after thermal sintering

Nickel and silica nanoparticles help to fill voids, particularly after the thermal sintering process. The porosity decreases after sintering because the atoms are closer together, due to the cermet compounds' atoms being close to each other. The sintering temperature significantly aids in filling the voids formed during the pressing process [51].

6.4. Brinell hardness results

Fig. 5 shows the correlation between the volumetric reinforcement ratios of silica and the Brinell hardness before and after sintering at 1100 °C for two hours. It is evident that the hardness gradually increases with the addition ratios of SiO_2 , demonstrating the significant impact of nanomaterials on nickel. The highest hardness, reaching 745 kg/mm², occurs at a reinforcement percentage of 10 %.

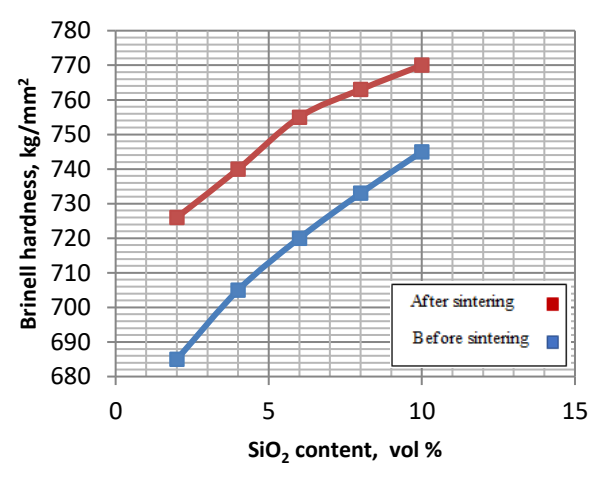


Fig. 5. The relationship between the reinforcement volumetric ratios and Brinell hardness before and after thermal sintering

This is attributed to agglomeration of the reinforced material, which negatively affects hardness and hinders mechanical crosslinking between the atoms of the base and cementing materials [52]. After sintering, we observe a

notable rise in hardness with the addition ratios. The maximum hardness of (770 kg/mm²) is achieved at the 10 % SiO₂ ratio. This increase is primarily due to the heat level, which promotes atom bonding and cohesion, leading to enhanced fusion strength, reduced porosity, and increased hardness and durability of the nickel oxide phase. Furthermore, the presence of nickel oxide serves as a secondary support phase that contributes to improved mechanical properties [53].

6.5. Diagonal compressive strength results

Fig. 6 shows the relationship between the change in the volumetric ratios of nano-silica and the compressive strength before and after the thermal sintering process. The figure shows that as the volumetric ratios increased, the compressive strength also increased. For instance, the compressive strength rose from 34-52 MPa when the silica content was 2% to 10% before sintering.

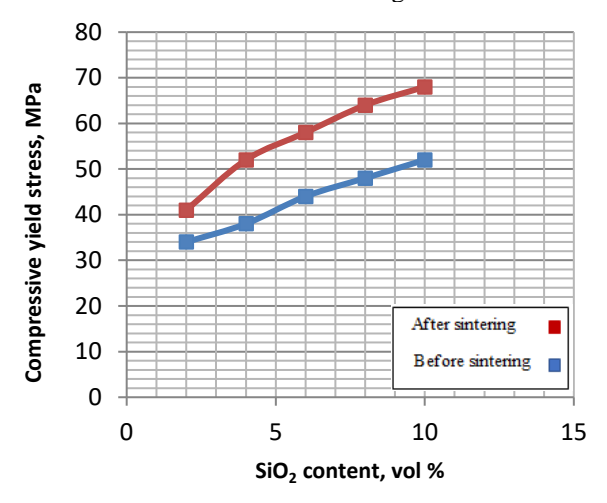


Fig. 6. The relationship between the volumetric reinforcement ratios and the radial compressive strength before and after thermal sintering

Additionally, after the thermal sintering process, the compressive strength of the diameter increased from 41-68 MPa at a silica content of 2 % to 10 %. The higher compressive strength is also due to the strong particle reinforcement and the mixing of ceramic material with metal, resulting in a hard cermet compound [54]. This process also leads to the formation of nickel sintering, which effectively resists local deformations, and ultimately creates cohesive samples with high compressive strength. The high sintering temperature for two hours plays a crucial role in enhancing the bonding strength between the particles of the overlay components. This is achieved through effective spreading and distribution, leading to increased density and reduced porosity after sintering. Consequently, this supports and reinforces the overlay mass by effectively filling the voids between the surface atoms, resulting in a cohesive and strong overlay [55]. The Young's modulus is influenced by the material type and its ability to maintain a constant ratio between stress area and strength when subjected to an applied load by reducing the Young's modulus, and increasing the amount of silica up to 10 % SiO2, we achieved a high Young's modulus, indicating low material deformation and requiring significant force to change its shape. This transformation creates a hard cement compound with high load-bearing strength [56-58].

7. CONCLUSIONS

The current article suggests the potential for merging nano-ceramic powders with nickel metal, resulting in strengthened nickel with high mechanical specifications. This was achieved through standard thermal sintering at 1000 °C and a 10 % addition of SiO₂, leading to improved diagonal hardness and compressive resistance, as well as reduced porosity. Additionally, X-ray diffraction examination revealed the presence of cubic nickel oxide, while scanning electron microscope results showed an intertwined crystalline structure with a distinct surface under these optimal conditions.

REFERENCES

- Neikov, O.D., Yefimov, N.V. Handbook of Non-Ferrous Metal Powders: Technologies and Applications. Elsevier, Amsterdam, 2009: pp. 14-20.
- Suchanek, W.L., Riman, R.E. Hydrothermal Synthesis of Advanced Ceramic Powders Advances in Science and Technology 45 2006: pp. 184–193. https://doi.org/10.4028/www.scientific.net/AST.45.184
- 3. **Tahara, K.** Pharmaceutical Formulation and Manufacturing Using Particle/Powder Technology for Personalized Medicines *Advanced Powder Technology* 31 (1) 2020: pp. 387 392. https://doi.org/10.1016/j.apt.2019.10.031
- Duran, J. Sands, Powders, and Grains: An Introduction to the Physics of Granular Materials. Springer, New York, 2012: pp. 24-29.
- Marinho, B., Ghislandi, M., Tkalya, E., Koning, C.E., de With, G. Electrical Conductivity of Compacts of Graphene, Multi-Wall Carbon Nanotubes, Carbon Black, and Graphite Powder Powder Technology 221 2012: pp. 351 358. https://doi.org/10.1016/j.powtec.2012.01.024
- Liu, H., Cheng, X., Chong, Y., Yuan, H., Huang, J.Q.,
 Zhang, Q. Advanced Electrode Processing of Lithium Ion Batteries: A Review of Powder Technology in Battery Fabrication *Particuology* 57 2021: pp. 56–71. https://doi.org/10.1016/j.partic.2020.12.003
- 7. **Iams, A.D., Gao, M.Z., Shetty, A., Palmer, T.A.** Influence of Particle Size on Powder Rheology and Effects on Mass Flow during Directed Energy Deposition Additive Manufacturing *Powder Technology* 396 2022: pp. 316–326. https://doi.org/10.1016/j.powtec.2021.10.059
- 8. **Wani, T.A., Ganesh, S.** Study on Fresh Properties, Mechanical Properties and Microstructure Behavior of Fiber Reinforced Self Compacting Concrete: A Review *Materials Today: Proceedings* 62 2022: pp. 6663 6670. https://doi.org/10.1016/j.matpr.2022.04.666
- 9. **Ujah, C.O., Kallon, D.V.V.** Trends in Aluminium Matrix Composite Development *Crystals* 12 (10) 2022: pp. 1357. https://doi.org/10.3390/cryst12101357
- Lehmhus, D., Busse, M., Herrmann, A., Kayvantash, K. Structural Materials and Processes in Transportation. John Wiley and Sons, India, 2013: pp. 4–8.
- 11. Wang, J.L., Li, Y.Q., Byon, Y.J., Mei, S.G., Zhang, G.L. Synthesis and Characterization of NiTiO₃ Yellow Nano

- Pigment with High Solar Radiation Reflection Efficiency *Powder Technology* 235 2013: pp. 303 306. https://doi.org/10.1016/j.powtec.2012.10.044
- 12. **Lin, Z., Chi, S., Ye, J., Zhu, Z., Li, Y., Jin, Y.** Effect of Liquid Layer on the Motion of Particle during Oblique Wet Collision *Advanced Powder Technology* 32 (9) 2021: pp. 3259–3267. https://doi.org/10.1016/j.apt.2021.07.011
- Jiang, X., Overman, N., Smith, C., Ross, K. Microstructure, Hardness and Cavitation Erosion Resistance of Different Cold Spray Coatings on Stainless Steel 316 for Hydropower Applications *Materials Today Communications* 25 2020: pp. 101305. https://doi.org/10.1016/j.mtcomm.2020.101305
- Ramirez-Coretti, A., Eckelman, C.A., Wolfe, R.W. Inorganic-Bonded Composite Wood Panel Systems for Low-Cost Housing: A Central American Perspective Forest Products Journal 48 (4) 1998: pp. 63.
- Castelo, A.M.P. Emergency Constructions in Catastrophe Affected Regions. Development of a Constructive Solution in Advanced Composite Materials. MSc Dissertation, University of Lisbon (2014). (In Portuguese)
- Suib, S.L. A Review of Nanoceramic Materials for Use in Ceramic Matrix Composites. In Sol-gel Based Nanoceramic Materials: Preparation, Properties and Applications. Elsevier, 2017: pp. 185 – 230. https://doi.org/10.1007/978-3-319-49512-5_7
- 17. Fu, S., Liu, X., Jin, J., Zhang, Z., Liu, Y., Yan, M. Magnetic Properties Evolution with Grain Boundary Phase Transformation and Their Growth in Nd-Fe-Cu-Ga-B Sintered Magnet during Post-Sinter Annealing Process Intermetallics 137 2021: pp. 107303. https://doi.org/10.1016/j.intermet.2021.107303
- Hosseini, E., Popovich, V.A. A Review of Mechanical Properties of Additively Manufactured Inconel 718 Additive Manufacturing 30 2019: pp. 100877. https://doi.org/10.1016/j.addma.2019.100877
- 19. Lin, K., Nie, G., Sheng, P., Zhao, S., Wu, S. Effects of Doping Al-Metal Powder on Thermal, Mechanical and Dielectric Properties of AlN Ceramics Ceramics International 48 (24) 2022: pp. 36210 36217. https://doi.org/10.1016/j.ceramint.2022.08.178
- Kaledin, A., Shikunov, S., Komarov, K., Straumal, B., Kurlov, V. SiC-Based Composite Material Reinforced with Molybdenum Wire *Metals* 13 (2) 2023: pp. 313. https://doi.org/10.3390/met13020313
- 21. Girimurugan, R., Maheskumar, P., Sahoo, G., Sivalingam, A., Mayakannan, S. Effect of Nano Alumina Powder and Water Hyacinth Stem Powder Addition on Tensile Properties of Polypropylene Matrix Hybrid Composites An Experimental Study Materials Today: Proceedings 60 2022: pp. 2099–2104. https://doi.org/10.1016/j.matpr.2022.01.477
- Peng, J., Yi, M., Sun, H., Xu, Y., Xiao, G., Chen, Z., Xu, C. Synthesis and Characterization of Mo and Ni Core-Shell Composite Powder-Reinforced (W, Ti)C-Based Cermet *Materials Today Communications* 31 2022: pp. 103749. https://doi.org/10.1016/j.mtcomm.2022.103749
- Ekaputra, C.N., Weiss, D., Mogonye, J.E., Dunand, D.C. Eutectic, Precipitation-Strengthened Alloy via Laser Fusion of Blends of Al-7Ce-10Mg (wt.%), Zr, and Sc Powders Acta Materialia 246 2023: pp. 118676. https://doi.org/10.1016/j.actamat.2023.118676
- 24. Xi, L., Feng, L., Gu, D., Prashanth, K.G., Kaban, I., Wang, R., Eckert, J. Microstructure Formation and Mechanical Performance of Micro-Nanoscale Ceramic

- Reinforced Aluminum Matrix Composites Manufactured by Laser Powder Bed Fusion *Journal of Alloys and Compounds* 2023: pp. 168803.
- https://doi.org/10.1016/j.jallcom.2023.168803
- Bakshi, S.R., Lahiri, D., Agarwal, A. Carbon Nanotube Reinforced Metal Matrix Composites – A Review International Materials Reviews 55 (1) 2010: pp. 41 – 64. https://doi.org/10.1179/095066009X12572530170543
- 26. **Sahoo, B.P., Das, D.** Investigation on Reinforcement Incorporation Factor and Microstructure of Al 7075/Submicron-TiB₂ Metal Matrix Composites Processed Through a Modified Liquid Metallurgy Technique *Experimental Techniques* 45 (2) 2021: pp. 179–193. https://doi.org/10.1007/s40799-020-00429-x
- 27. Lv, S., Zu, Y., Chen, G., Zhao, B., Fu, X., Zhou, W. A Multiple Nonmetallic Atoms Co-Doped CrMoNbWTi Refractory High-Entropy Alloy with Ultra-High Strength and Hardness Materials Science and Engineering: A 795 2020: pp. 140035. https://doi.org/10.1016/j.msea.2020.140035
- Mussatto, A., Ahad, I.U., Mousavian, R.T., Delaure, Y., Brabazon, D. Advanced Production Routes for Metal Matrix Composites *Engineering Reports* 3 (5) 2021: pp. e12330. https://doi.org/10.1002/eng2.12330
- Nurhudan, A.I., Supriadi, S., Whulanza, Y., Saragih, A.
 S. Additive Manufacturing of Metallic Based on Extrusion Process: A Review *Journal of Manufacturing Processes* 66 2021: pp. 228 – 237. https://doi.org/10.1016/j.jmapro.2021.04.018
- Salih, W.A., Allah, S.M.A., Darweesh, S.Y. Effect of spray angle on some physical properties of a ceramic system produced by thermal spraying coating Al-Bahir Journal for Engineering and Pure Sciences 2 (2) 2023: pp. 4 https://doi.org/10.55810/2313-0083.1022
- 31. **Negi, S., Mishra, V., Ror, C.K., Sharma, R.K.** Laser Powder Bed Fusion of Glass-Filled Polyamide-Composite with Enhanced Physical Properties *Journal of Reinforced Plastics and Composites* 42 (23 24) 2023: pp. 1303 1320. https://doi.org/10.1177/07316844231152602
- Letenneur, M., Brailovski, V., Kreitcberg, A., Paserin, V., Bailon-Poujol, I. Laser Powder Bed Fusion of Water-Atomized Iron-Based Powders: Process Optimization Journal of Manufacturing and Materials Processing 1 (2) 2017: pp. 23. https://doi.org/10.3390/jmmp1020023
- 33. **Fereiduni, E., Ghasemi, A., Elbestawi, M.** Selective Laser Melting of Hybrid Ex-Situ/In-Situ Reinforced Titanium Matrix Composites: Laser/Powder Interaction, Reinforcement Formation Mechanism, and Non-Equilibrium Microstructural Evolutions *Materials and Design* 184 2019: pp. 108185. https://doi.org/10.1016/j.matdes.2019.108185
- 34. **Mohammad, S., Patra, S., Harichandan, B.** Reductants in Iron Ore Sintering: A Critical Review *Fuel* 332 2023: pp. 126194. https://doi.org/10.1016/j.fuel.2022.126194
- 35. Chirayil, C.J., Abraham, J., Mishra, R.K., George, S.C., Thomas, S. Instrumental Techniques for the Characterization of Nanoparticles Thermal and Rheological Measurement Techniques for Nanomaterials Characterization 2017: pp. 1 36. https://doi.org/10.1016/B978-0-323-46139-9.00001-3
- 36. **Ali, A., Chiang, Y.W., Santos, R.** X-Ray Diffraction Techniques for Mineral Characterization: A Review for

- Engineers of the Fundamentals, Applications, and Research Directions *Minerals* 12 (2) 2022: pp. 205. https://doi.org/10.3390/min12020205
- 37. Zhang, X., Xu, J., Qian, Y., Zuo, J., Zhang, Z., Li, M. Synthesis and Characterisation of Novel Single-Phase HfCxN1-x Ceramic Powders Materials Chemistry and Physics 295 2023: pp. 127099. https://doi.org/10.1016/j.matchemphys.2022.127099
- 38. Vakifahmetoglu, C., Semerci, T., Soraru, G.D. Closed Porosity Ceramics and Glasses *Journal of the American Ceramic Society* 103 (5) 2020: pp. 2941–2969. https://doi.org/10.1111/jace.16934
- 39. Sun, X., Kuwik, B.S., Yang, Q., Chocron, S., Hurley, R.C., Haber, R.A., Ramesh, K.T. Effects of Particle Size, Shape and Loading Rate on the Normal Compaction of an Advanced Granular Ceramic Powder Technology 2023: pp. 118243. https://doi.org/10.1016/j.powtec.2023.118243
- 40. Obada, D.O., Dauda, E.T., Abifarin, J.K., Dodoo-Arhin, D., Bansod, N.D. Mechanical Properties of Natural Hydroxyapatite Using Low Cold Compaction Pressure: Effect of Sintering Temperature Materials Chemistry and Physics 239 2020: pp. 122099. https://doi.org/10.1016/j.matchemphys.2019.122099
- 41. **Karim, A.S., Majeed, Z.N., Darweesh, S.Y.** The Effect of Nanostructured Zirconia Reinforcement on the Mechanical and Structural Properties of a Copper-Based System *In Materials Science Forum* 1039 2021: pp. 297–306. https://doi.org/10.4028/www.scientific.net/MSF.1039.297
- 42. Katok, O.A., Muzyka, M.R., Shvets, V.P., Sereda, A.V., Kharchenko, V.V., Bisyk, S.P. Determination of Hardness of High-Strength Steels by the Brinell Method: Part 1. Improvement of Measurement Accuracy Strength of Materials 53 (6) 2021: pp. 902 908. https://doi.org/10.1007/s11223-022-00358-7
- Nguyen, M.H., Trinh, S.H., Ly, H.B. Toward Improved Prediction of Recycled Brick Aggregate Concrete Compressive Strength by Designing Ensemble Machine Learning Models Construction and Building Materials 369 2023: pp. 130613. https://doi.org/10.1016/j.conbuildmat.2023.130613
- 44. **Lan, G., Weng, G., Zhang, K.** Assessment of Optimal Specimen to Measure the Compressive Strength of Earthen-Based Masonry *Measurement* 208 2023: pp. 112484. https://doi.org/10.1016/j.measurement.2023.112484
- 45. Bahtiar, E.T., Imanullah, A.P., Hermawan, D., Nugroho, N. Structural Grading of Three Sympodial Bamboo Culms (Hitam, Andong, and Tali) Subjected to Axial Compressive Load Engineering Structures 181 2019: pp. 233 245. https://doi.org/10.1016/j.engstruct.2018.12.026
- 46. Pei, X., Yi, S., Zhao, Y., Mu, Y., Yu, Y., Cui, M., Zhang, Y. Nickel Oxide Nanoparticles Dispersed on Biomass—Derived Amorphous Carbon/Cobalt Silicate Support Accelerate the Oxygen Evolution Reaction *Journal of Colloid and Interface Science* 616 2022: pp. 476–487. https://doi.org/10.1016/j.jcis.2022.02.078
- 47. Tahmasbi, L., Sedaghat, T., Motamedi, H., Kooti, M. Mesoporous Silica Nanoparticles Supported Copper (II) and Nickel (II) Schiff Base Complexes: Synthesis, Characterization, Antibacterial Activity and Enzyme Immobilization Journal of Solid State Chemistry 258 2018: pp. 517 525.

https://doi.org/10.1016/j.jssc.2017.11.015

- 48. **Ghazal, N.A., Majeed, Z.N., Darweesh, S.Y.** The Effect Of Adding Different Percentages Manganese on Some Mechanical and Magnetic Properties of Composite (Al-Cu) *AIP Conference Proceedings* 2885 (1) 2024: pp. 040003. https://doi.org/10.1063/5.0182248
- 49. **Salih, E.J., Allah, S.M.A., Darweesh, S.Y.** Study the Structural and Mechanical Properties of the Cu-WC Composite *AIP Conference Proceedings* 2398 (10) 2022: pp. 020035. https://doi.org/10.1063/5.0094030
- 50. Vázquez, O.F.G., Reyes, C.F., Morales, M.O., Kamaraj, S.K., Virgen, M.D.R.M., Montoya, V.H. Facile Scalable Manufacture of Improved Electrodes Using Structured Surface Coatings of Nickel Oxide as Cathode and Reduced Graphene Oxide as Anode for Evaluation in a Prototype Development on Microbial Fuel Cells International Journal of Hydrogen Energy 47 (70) 2022: pp. 30248 30261. https://doi.org/10.1016/j.ijhydene.2022.06.311
- 51. Fang, Y., Chen, N., Du, G., Zhang, M., Zhao, X., Cheng, H., Wu, J. High-Temperature Oxidation Resistance, Mechanical and Wear Resistance Properties of Ti(C,N)-Based Cermets with Alo.3CoCrFeNi High-Entropy Alloy as a Metal Binder *Journal of Alloys and Compounds* 815 2020: pp. 152486. https://doi.org/10.1016/j.jallcom.2019.152486
- Kumar, S.S., Raja, V.M. Processing and Determination of Mechanical Properties of Prosopis Juliflora Bark, Banana and Coconut Fiber Reinforced Hybrid Bio Composites for an Engineering Field *Composites Science and Technology* 208 2021: pp. 108695. https://doi.org/10.1016/j.compscitech.2021.108695
- 53. Wegener, T., Koopmann, J., Richter, J., Krooß, P., Niendorf, T. CuCrZr Processed by Laser Powder Bed Fusion Processability and Influence of Heat Treatment on Electrical Conductivity, Microstructure and Mechanical Properties Fatigue and Fracture of Engineering Materials and Structures 44 (9) 2021: pp. 2570 2590. https://doi.org/10.1111/ffe.13527
- 54. Zhang, Q., Cheng, Y., Chen, B., Liang, S., Zhuo, L. Microstructure and Properties of W–25 wt% Cu Composites Reinforced with Tungsten Carbide Produced by an In Situ Reaction *Vacuum* 177 2020: pp. 109423. https://doi.org/10.1016/j.vacuum.2020.109423
- 55. Ahmed, M.N., Daham, N.A., Darweesh, S.Y. Structural and Mechanical Properties for (Ni-WC) System by Using Thermal Spray AIP Conference Proceedings 2885 (1) 2024: pp. 020013. https://doi.org/10.1063/5.0181722
- Antar, R.S., Darweesh, S.Y., Ridha, F.W. Production of a Double Cermet Coating to Treatment of the Turbine Blades Engineering Research Express 6 (1) 2024: pp. 015407. https://doi.org/10.1088/2631-8695/ad2f82
- 57. Humeedi, S.H., Abdulkareem, S.M., Darweesh, S.Y. The synthetic and mechanical properties of a silica matrix cermet composite *Journal of Wuhan University of Technology-Mater. Sci. Ed.* 37 (3) 2022: pp. 423 428. https://doi.org/10.1007/s11595-022-2548-5
- 58. **Ibraheem, A.M.,** Allah, S.M.A., Darweesh, S.Y. Enhancement the Properties of Aluminum by Adding Boron Carbide by the Powder Method *Journal of Physics: Conference Series* 1999 (1) 2021: pp. 012074. https://doi.org/10.1088/1742-6596/1999/1/012074



© Hassan et al. 2026 Open Access This article is distributed under the terms of the Creative Commons Attribution 4.0 International License (http://creativecommons.org/licenses/by/4.0/), which permits unrestricted use, distribution, and reproduction in any medium, provided you give appropriate credit to the original author(s) and the source, provide a link to the Creative Commons license, and indicate if changes were made.